Image and Vision Computing 28 (2010) 1671–1681

Contents lists available at ScienceDirect

Image and Vision Computing

journal homepage: www.elsevier.com/locate/imavis

Iris segmentation in non-ideal images using graph cuts

Shrinivas Pundlik *, Damon Woodard, Stan Birchfield

Clemson University, Clemson, SC 29634, USA

ARTICLE INFO

Article history:
Received 4 October 2009
Received in revised form 16 April 2010
Accepted 16 May 2010

Keywords:
Iris segmentation
Graph cuts
Starburst

ABSTRACT

A non-ideal iris image segmentation approach based on graph cuts is presented that uses both the appearance and eye geometry information. A texture measure based on gradients is computed to discriminate between eyelash and non-eyelash regions, combined with image intensity differences between the iris, pupil, and the background (region surrounding the iris) are utilized as cues for segmentation. The texture and intensity distributions for the various regions are learned from histogramming and explicit sampling of the pixels estimated to belong to the corresponding regions. The image is modeled as a Markov Random Field and the energy minimization is achieved via graph cuts to assign each image pixel one of the four possible labels: iris, pupil, background, and eyelash. Furthermore, the iris region is modeled as an ellipse, and the best fitting ellipse to the initial pixel based iris segmentation is computed to further refine the segmented region. As a result, the iris region mask and the parameterized iris shape form the outputs of the proposed approach that allow subsequent iris recognition steps to be performed for the segmented irises. The algorithm is unsupervised and can deal with non-ideality in the iris images due to out-of-plane rotation of the eye, iris occlusion by the eyelids and the eyelashes, multi-modal iris grayscale intensity distribution, and various illumination effects. The proposed segmentation approach is tested on several publicly available non-ideal near infra red (NIR) iris image databases. We compare both the segmentation error and the resulting recognition error with several leading techniques, demonstrating significantly improved results with the proposed technique.

1. Introduction

The human iris has emerged as an effective biometric modality due to its uniqueness, stability and secure nature (being an internal organ, it is difficult to replace or remove thus making it more difficult to spoof the system). Automated person identification and verification systems based on the iris biometric have become increasingly popular over the past few years due to the availability of efficient and accurate iris recognition algorithms. However, most iris recognition approaches rely on *ideal iris images* for accurate recognition, i.e., low noise iris images in which the person is looking straight at the camera. The performance of an iris recognition system degrades if the iris undergoes large occlusion by eyelids and eyelashes, illumination changes, or out-of-plane rotation. These constraints on the input images require a significant amount of user cooperation during image acquisition, thereby limiting the application domain of iris recognition systems. Fig. 1 depicts an example of an ideal and non-ideal iris images. Iris recognition using such *non-ideal iris images* is a challenging problem which impacts the application of iris recognition as a means of personal identification. In this paper, we present an algorithm to segment non-ideal iris images, specifically, images that are captured by a near infra red (NIR) camera, and in which the iris regions are affected by occlusion by eyelids and eyelashes, illumination artifacts, blurring, and out-of-plane rotation.

In previous work, geometric approaches to iris segmentation have been common. For example, in his pioneering work on iris recognition, Daugman [8,9] describes an integro-differential approach where a circle and parabolic curves are respectively fitted to the iris and above and below the iris to account for eyelids and eyelashes. In a competing approach, Wildes [29] uses binary edge images for detecting iris regions. Similarly, geometric cues such as pupil location or eyelid location have been used for iris localization [11], while stretching and contraction properties of the pupil and iris have also been used [14]. Another important approach has been to detect the eyelashes in order to determine iris occlusion. To this end, Ma et al. [20,21] use Fourier transforms to determine whether the iris is being occluded by the eyelashes; the unique spectrum associated with eyelashes is used to reject images in which significant iris occlusion occurs. Other approaches for eyelash segmentation involve the use of image intensity differences between the eyelash and iris regions [10,16,17], gray level co-occurrence matrices [1], and the use of multiple eyelash models [30]. A comprehensive literature review of research in iris segmentation and recognition can be found in [2].

The application of these iris segmentation techniques is limited to ideal iris images, assuming that the shape of the iris can be modeled as a circle. Such a simplifying assumption limits the range of input

* Corresponding author.
E-mail addresses: spundli@clemson.edu (S. Pundlik), woodard@clemson.edu (D. Woodard), stb@clemson.edu (S. Birchfield).

0262-8856/$ – see front matter © 2010 Elsevier B.V. All rights reserved.
doi:10.1016/j.imavis.2010.05.004

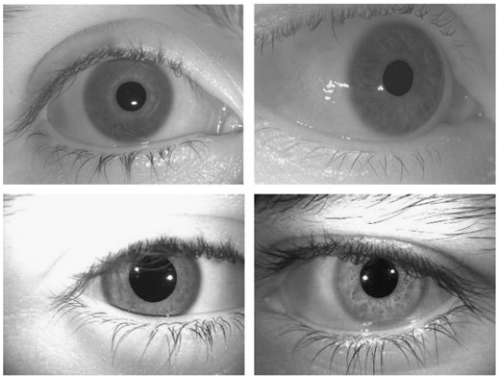

Fig. 1. An ideal iris image (top left), and iris images of varying quality, containing out-of-plane rotation, illumination effects, and occlusion.

images that can be successfully used for recognition. By relying heavily on eye geometry, these techniques are sensitive to image noise and the variations in the iris shape due to out-of-plane rotation and occlusions. Recently, it has been proposed that iris segmentation with higher degrees of freedom leads to an improved recognition performance. To this effect, some more recent approaches to handle non-ideal iris images rely upon active contour models [10] or geodesic active contours [24,26] for iris segmentation. Schuckers et al. [25] describe an approach for iris recognition in off-angle images. Another recent approach described in [28] segments the iris region using curve evolution strategy. We have recently proposed a graph cuts based algorithm for eyelash and iris segmentation [23]. With this approach, the eye is modeled as a Markov Random Field and graph cuts are used to minimize an objective function that enforces spatial continuity in the region labels found. Four labels are assigned: iris, pupil, eyelashes, and background, in addition to specular reflections. By automatically choosing the expected gray level values of the via histogramming, the algorithm adapts to variations in images, enabling it to handle non-ideal iris images containing out-of-plane rotation and extensive iris occlusion by eyelashes and eyelids.

In this paper we propose an alternative representation for the segmented iris region based on a combination of an appearance based pixel-level segmentation and an eye geometry based iris delineation. As an improvement over [23], the proposed approach incorporates explicit sampling of iris and background intensities in order to handle multi-modal intensity distributions which are commonly found in the non-ideal iris images. A RANSAC-based procedure is employed for robust iris refinement by estimating the elliptical boundary of the iris. Thus, the proposed approach effectively combines the image appearance and eye geometry information for iris segmentation and achieves a high degree of freedom as a result. Extensive experimental results on the WVU Non-Ideal and Off-Angle Iris image databases show the effectiveness of the proposed algorithm on iris images with illumination artifacts, occlusion and out-of-plane rotation. The paper is organized as follows. Section 3 provides a detailed formulation of the iris segmentation problem, followed by the proposed segmentation approach in Section 4 and the iris region refinement task in Section 5. The results of iris segmentation and recognition experiments using publicly available non-ideal iris image databases are presented in Section 6. Finally, suggestions for future work are provided.

2. Formulation

Let the iris be represented by an ellipse $\mathbf{s} = (x_s, y_s, a_s, b_s)$, where (x_s, y_s) is the center of the ellipse, and a_s and b_s are the lengths of the major and minor axes which are assumed to be aligned with the x and y axes. Similarly, let the pupil be represented by an ellipse $\mathbf{p} = (x_p, y_p, a_p, b_p)$. Both, $\mathbf{s}$ and $\mathbf{p}$ are parameterized assuming no in-plane rotation of the eye. We make this assumption because i) out-of-plane rotation of the eye leads to the distortion of the iris shape in the captured image, and ii) the images that we deal with in this work, out-of-plane rotation of the eye is more frequently observed than a significant in-plane rotation. A segmentation ψ: $\mathbf{x} \rightarrow \ell$ assigns to every pixel $\mathbf{x}$ in an image I one of four values, $\ell \in \mathcal{L} =$ {iris, pupil, eyelash, background}, indicating the region of the eye corresponding to the pixel. Our goal is to estimate these parameters $\Theta = \langle \mathbf{s}, \mathbf{p}, \psi \rangle$ from a single image:

$$p(\Theta|I) = p(s|\mathbf{p}, \psi, I)p(\mathbf{p}|\psi, I)p(\psi|I). \tag{1}$$

Although there is a high degree of dependency between the ellipses and segmentation, it is important to retain both in the formulation in order to enable accurate estimation in the presence of noise, as we shall see.

From Bayes' rule, the segmentation term can be decomposed as $\log p(\psi|I) \propto \log p(I|\psi) + \log p(\psi)$. Expressed in terms of Gibbs energy, our goal is to minimize

$$E(\psi) = E_D(I|\psi) + \lambda E_S(\psi), \tag{2}$$

where E_D is the data term and E_S enforces an *a priori* piecewise smoothness assumption. Assuming a Markov Random Field (MRF), these terms are given by

$$E_D(\psi) = \sum_{n=1}^{N} D_n(\ell_n) \tag{3}$$

$$E_S(\psi) = \sum_{n=1}^{N} \sum_{m \in \mathcal{N}_s(n)} S_{m,n}(\ell_m, \ell_n), \tag{4}$$

where ℓ_n is the label of pixel n, N is the total number of pixels in the image, $\mathcal{N}_s(n)$ is the neighborhood of pixel n, and λ is the regularization parameter. In the sections that follow, we describe a procedure for minimizing the functional using the technique of graph cuts, as well as for determining the data and smoothness terms from the iris image. Then we show how to fit the pupil and iris ellipses based on this segmentation.

An overview of our approach is presented in Fig. 2. The first step is a preprocessing procedure applied to the input images to deal with specular reflections and low contrast which may cause errors in segmentation. In the second step we perform iris segmentation using texture and grayscale intensity using an energy minimization procedure that employs graph cuts to produce a labeling of the image separating the pupil, iris, eyelash, and background pixels. The iris refinement step involves fitting ellipses to the segmented iris regions to prune erroneous regions if present. This step produces a binary mask of the iris pixels between the estimated ellipses along with the ellipse parameters. The final step is to combine the iris region mask and the specular reflection mask (removing the specular reflections from the iris region mask denoted by binary subtraction) to output usable iris regions, which along with the ellipse describing the iris region, can then used for recognition. These steps are described in more detail in the following sections.

3. Segmentation

The segmentation of the image proceeds by classifying the pixels according to their texture and intensity in a graph cut framework. In this section, we explain our approach to learn the texture and grayscale intensity distributions for the various segments i.e., eyelash, iris, pupil and background, as well as using this information in a graph cuts framework for segmentation. Prominent issues to be addressed while preprocessing include image noise, low contrast, and specular reflections. Image smoothing and contrast correction are employed to deal with the former two issues. A Gaussian kernel of size 3×3 is used

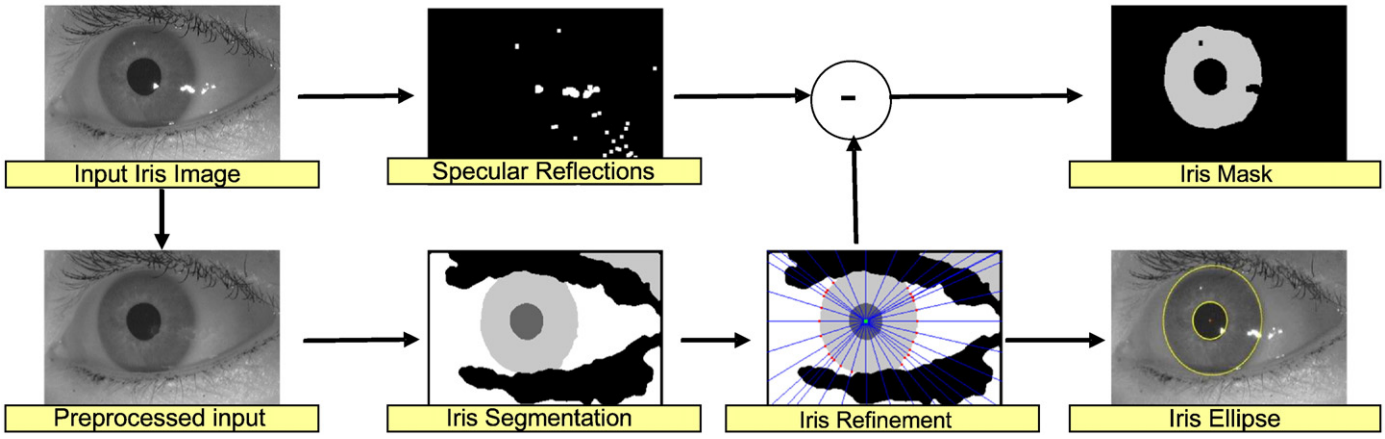

Fig. 2. Overview of the proposed approach.

for smoothing the input image. Low contrast images are subjected to gamma correction (gamma value set at 1.5) to improve contrast. Our approach for dealing with specular reflections is described in [23] and is similar to the approaches used in [5,15,19,25], where we detect these pixels by simply thresholding the image with a high threshold. Pixels above the threshold are set to invalid and are not used during recognition. For further segmentation, we construct a preprocessed image by filling in the invalid pixels iteratively using a nearest neighbor-based interpolation procedure.

3.1. Texture computation

Occlusion of the iris region by eyelashes and eyelids is one of the main causes of the images being non-ideal. When eyelashes occlude the iris, they not only negatively affect the estimation of the shape of the iris, but they also corrupt pixels that otherwise would be used in the recognition process. Previous approaches that are based on some variation of gray level thresholding will not be effective in non-ideal images due to extreme illumination variation. To detect eyelashes, we use the characteristic that they are textured. The goal is not so much to compute the precise texture for discrimination as it is done during iris recognition, but to establish a coarse texture measure that can discriminate between eyelash and non-eyelash regions. Let I_x and I_y denote the derivatives of the image in the x and y directions, respectively. The texture of a pixel n is computed using two measures. First, the Hessian captures the intensity variation in orthogonal directions [27]:

$$H(n) = \sum_{m \in \mathcal{N}_g(n)} \begin{bmatrix} I_x^2(m) & I_x(m)I_y(m) \\ I_x(m)I_y(m) & I_y^2(m) \end{bmatrix}, \tag{5}$$

$n = 1,\ldots,N$, where $\mathcal{N}_g(n)$ is the local neighborhood around the pixel. If both the eigenvalues of $H(n)$ are large, then this is indicative of a high amount of texture in the region, leading to the measure $\mathcal{T}_h(n) = \min\{\lambda_1, \lambda_2\}$. To reduce the effects of noise, we threshold this measure as

$$\xi_\tau(\mathcal{T}_h(n)) = \begin{cases} \mathcal{T}_h(n) & \text{if } \mathcal{T}_h(n) > \tau \\ 0 & \text{otherwise} \end{cases}, \tag{6}$$

where τ is a preset threshold. While the Hessian captures pixels with large intensity variation in orthogonal directions, we also need to account for pixels for which the gradient changes in only a single direction. Therefore the second measure is based on the magnitude of the intensity gradient: $\mathcal{T}_g(n) = \sqrt{I_x^2(n) + I_y^2(n)}$. While we have found thresholding the Hessian measure to be necessary to achieve quality results, no such thresholding on the gradient magnitude is needed. Putting these measures together yields a measure of the texture of a pixel:

$$\mathcal{T}(n) = \frac{1}{2}\varphi(G_\sigma * \xi_\tau(\mathcal{T}_h(n))) + \frac{1}{2}\varphi(G_\sigma * \mathcal{T}_g(n)), \tag{7}$$

where G_σ is a 2D convolution kernel for smoothing the measures, and $\varphi(A(n)) = A(n)/\sum_n A(n)$ is a function that normalizes the Hessian and gradient magnitude values to enable them to be meaningfully added together. (Here A is an arbitrary function of n.) We use an isotropic Gaussian kernel with $\sigma = 5$. Fig. 3 shows the measures and the resulting texture map obtained for an iris image.

3.2. Intensity computation

Grayscale intensity of the various regions of the eye can also be effectively used for segmentation. However in the case of NIR images, while pupils are relatively easy to detect as dark regions, the intensities associated with the iris and background are much more difficult to model. Fig. 4 displays the intensity histograms of four iris images. The top row shows an ideal iris image, in which the optimal thresholds between pupil, iris, and background are easy to identify because there is little overlap between the regions. In the remaining non-ideal images, however, the iris and background regions interact in unpredictable ways: sometimes they overlap significantly, they

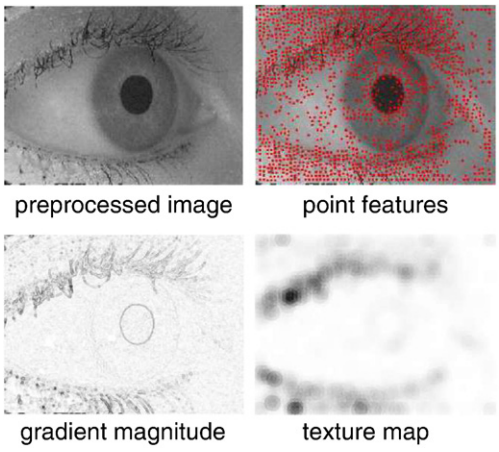

Fig. 3. Computation of texture in iris images to aid the separation of eyelash and non-eyelash parts. Thresholded Hessian (point features) and gradient magnitude are used for computing a texture map that shows the probability of each pixel belonging to the eyelash region (darker pixels indicate higher probability).

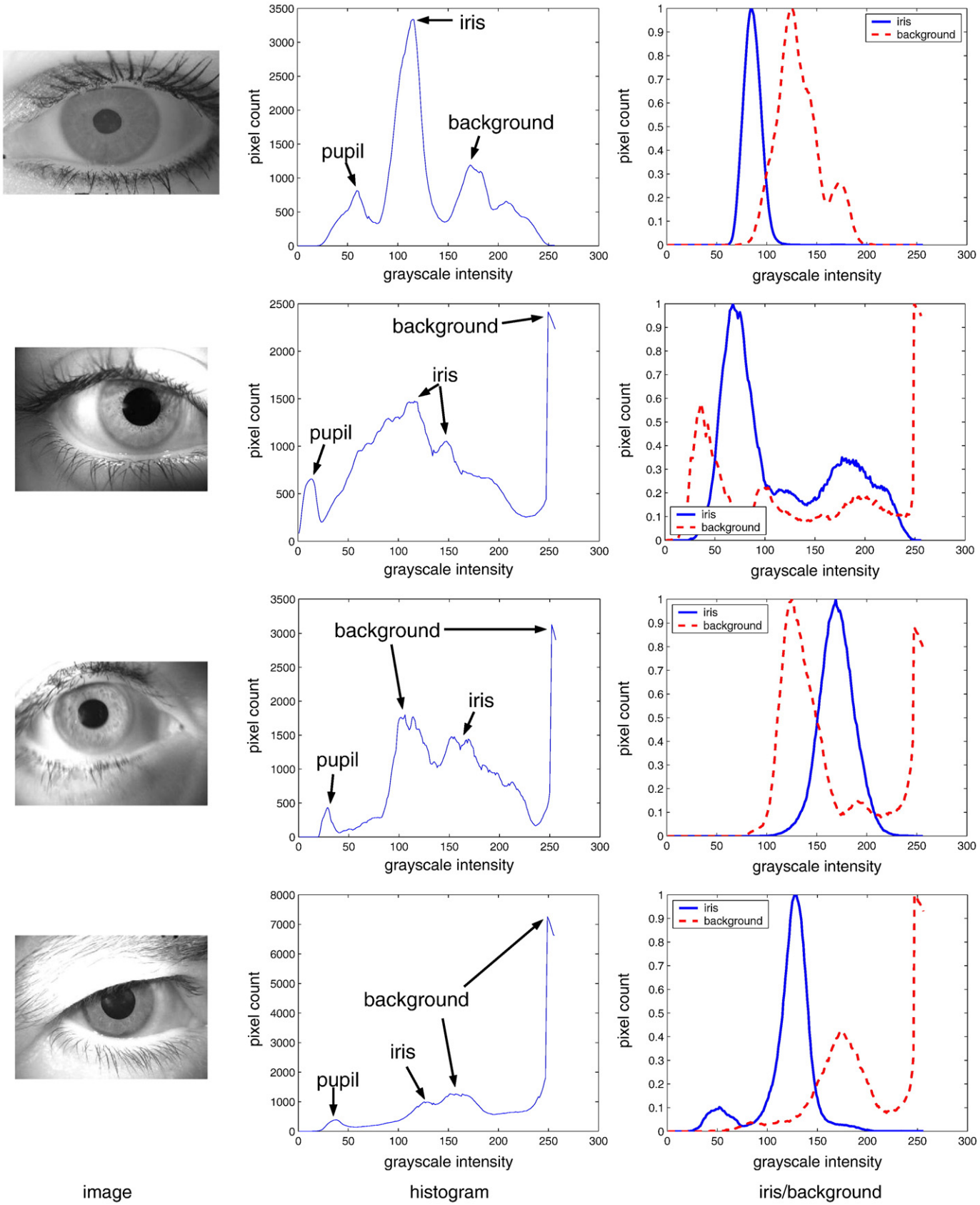

Fig. 4. Left: Four iris images. Middle: The intensity histogram of each image, with the pupil, iris, and background regions roughly identified. Right: Normalized histograms of the manually labeled iris (solid blue) and background (dashed red) pixels overlaid. Notice that the distributions of two regions exhibit significant overlap, multiple peaks, and unpredictable shape, thus making them not easily decipherable from the intensity histogram.

often exhibit multiple peaks, and occasionally they straddle one another. In the third row, for example, the background is both darker and brighter than the iris. From these data, we conclude that the intensity histogram alone is insufficient to determine the intensities associated with each region.

Our approach involves three steps. First, an initial pupil segmentation is determined by thresholding the image according to the first valley after the first initial peak in the intensity histogram. This straightforward procedure works well even if the overall image quality is poor, although it also may cause other dark regions to be mistakenly labeled as pupil. These errors are easily corrected by discarding small dark regions, then enforcing a minimum eccentricity on the remaining regions to distinguish the true pupil from the distractions.

The second step, shown in Fig. 5, is inspired by the Starburst algorithm used in eye tracking [18], in which the goal is to determine the eyegaze by locating the pupil center. In our case, the approximate location of the pupil center is already known from the previous step, and the goal is to estimate the iris boundary points. To this end, we extend rays outwards starting from the pupil center in all directions at one degree increments to detect the pupil/iris boundary (i.e., the first dark-to-light transition) as well as the iris/background boundary (i.e., the next intensity edge encountered). The pixels along each ray are classified as iris if they fall between the two boundaries, or as background if they lie beyond the outer boundary. While the first boundary can be detected reliably due to the low intensity of the pupil, the iris/background boundary is much more difficult to detect. Due to noise, rays may encounter intensity edges much sooner or later than the true boundary, leading to both false positives and false negatives in classifying pixels as iris. This problem is solved by calculating the median distance d_{med} along the rays to the boundary. For any ray whose boundary distance does not lie within $[\kappa d_{\text{med}}, d_{\text{med}}/\kappa]$, the boundary distance is set to d_{med}.

Once initial estimates for the iris and background regions have been thus obtained, the third step is to compute the expected intensity values of the various regions. To handle multi-modality, each region is modeled as a Gaussian mixture model (GMM):

$$C_{\ell}(n) = \sum_{i=1}^{K_{\ell}} \frac{(I(n)-\mu_{\ell,i})^2}{2\sigma_{\ell,i}^2}, \tag{8}$$

where $u_{\ell,i}$ and $\sigma_{\ell,i}$ are the mean intensity and standard deviation of the ith mixture component associated with region $\ell \in \mathcal{L}$. The component for $\ell =$ pupil is easily obtained from the original intensity histogram, as explained above. The components for $\ell =$ iris and $\ell =$ background are obtained by creating two new histograms from the initial estimates for the two regions, with only the background pixels that are within a certain radius of the iris considered. The mean shift algorithm ([6]) is applied to these histograms to detect peaks and valleys, which are then used to fit Gaussian approximations while enforcing a minimum distance between adjacent peaks. Because eyelash pixels tend to be textured, we use the texture measure to produce an initial segmentation, from which the expected intensities of these pixels is found in a similar manner.

3.3. Graph cuts segmentation

Now that we have a measure of the texturedness of each pixel, as well as a model for the expected intensities for each of the regions, we are in a position to solve for the segmentation of the image by minimizing the MRF of Eq. (2). An efficient and effective technique for such minimization is the multiway-cut algorithm [3,4]. The image can be considered as a weighted graph $G(V, E)$, where the vertices V are the pixels, and the edges E are the links between neighboring pixels. Additional nodes are added to the graph to be used as the source and sink in various iterations. These terminals correspond to the labels being assigned to the pixels. A cut is defined as a set of edges that separates the source and sink terminals, and the sum of the weights of the edges in the cut is the capacity of the cut. It can be shown that

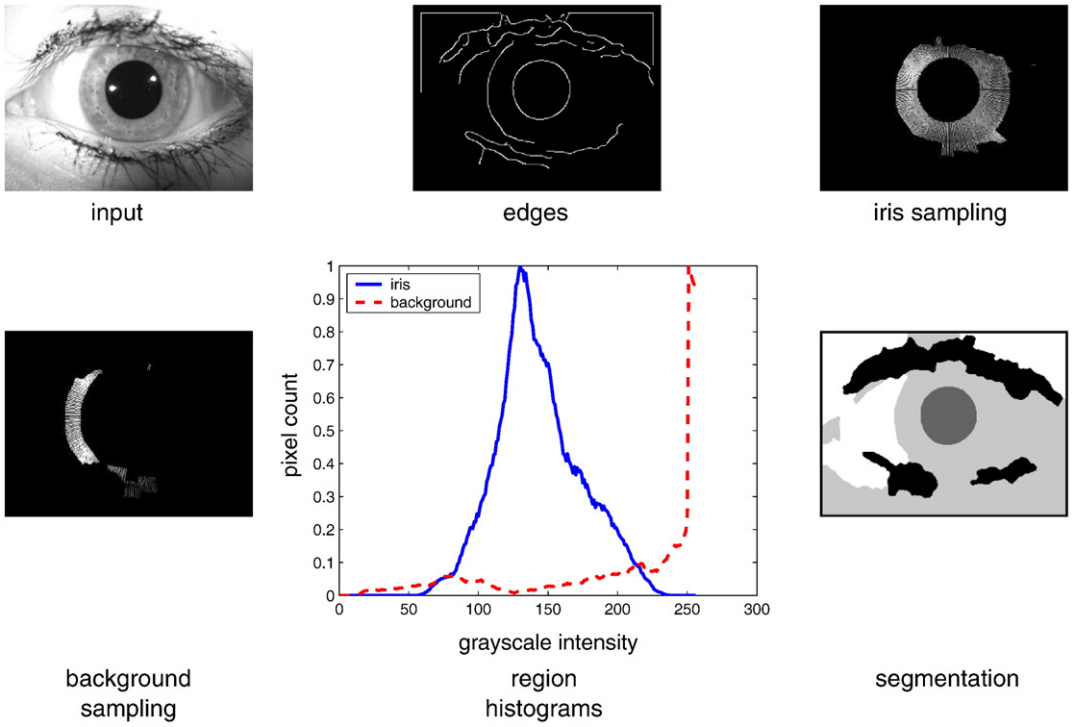

Fig. 5. Sampling iris and background regions for finding the corresponding intensity distributions. The Canny edge image (top center) is used to sample the estimated iris and background regions (top right and bottom left) and generate a histogram of pixel intensity distribution for those regions (bottom center). The peaks detected in these distributions are used as expected grayscale values in graph cuts for iris segmentation (bottom right).

finding the minimum cut, i.e., the cut with the minimum capacity, minimizes the Markov Random Field. Although this is an NP-hard problem, the solution provided by the $\alpha-\beta$ *swap* graph-cut algorithm [4] is in practice a close approximation to the global minimum. The algorithm works by initially assigning random labels to the pixels. Then for all possible pairs of labels, the pixels assigned to those labels are allowed to swap their label in order to minimize the energy of Eq. (2). The new labeling is retained only if the energy is minimized, and this procedure is repeated until the overall energy is not further minimized. Convergence is usually obtained in a few (about 3–4) iterations. Fig. 6 is a representative diagram showing the process of partitioning the input image.

The *t*-links in the graph connect the pixels to the labels. For pixel n, the weight of the *t*-link is given by

$$D_n(\ell_n) = \exp\{-(\mathcal{T}_\ell(n) + \eta C_\ell(n))\}, \tag{9}$$

where

$$\mathcal{T}_\ell(n) = \begin{cases} (\mathcal{T}(n)-1)^2 & \text{if } \ell = \textit{eyelash} \\ (\mathcal{T}(n))^2 & \text{otherwise.} \end{cases} \tag{10}$$

The expected texture value $\mathcal{T}(n)$ for a pixel belonging to an eyelash region is close to 1 while the texture value of a pixel belonging to one of the other regions is close to 0. In our experiments, we set $\eta = 0.6$. The *n*-links connect pixels with their neighbors and enforces piecewise smoothness in the result. The weight of the *n*-link of a pixel n is given by

$$S_{m,n}(\ell_m, \ell_n) = \exp\left\{-\|I(m)-I(n)\|^2\right\} \cdot \delta(\ell_m \neq \ell_n), \tag{11}$$

where $\delta(\cdot)$ is 1 if the condition is true or 0 otherwise. $I(m)$ and $I(n)$ are image intensities of mth and nth pixels, respectively. The condition set in function in $\delta(\cdot)$ assigns a weight to the *n*-link if the neighboring pixels have different labels and that weight is determined by the difference between the grayscale intensities between the two pixels.

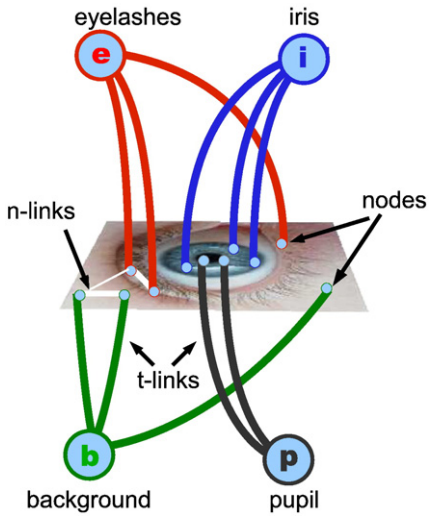

Fig. 6. Iris segmentation using graph cuts. The four terminals belong to the eyelash, iris, pupil and background regions while the image pixels are the nodes. Initially, all the terminals are connected to all the nodes with *t*-links while the nodes are connected to each other via *n*-links. The goal is to cut this graph such that a solution closest to optimum is obtained, where the nodes that remain connected at the end of the graph cuts procedure to the respective terminals are labels accordingly.

4. Iris region refinement

Now that a refined segmentation ψ has been computed, the pupil and iris ellipses can be estimated to maximize $p(\mathbf{s}|\mathbf{p}, \psi, I)$ and $p(\mathbf{s}|\mathbf{p}\psi, I)$. In this part of the algorithm, we use *a priori* information regarding the eye geometry for refining the segmentation of the iris region and overcoming errors due to noise and illumination effects. Specifically, we assume that the pupil and iris are well modeled as ellipses whose axes are aligned with the image axes, which is a reasonable approximation. Ellipses are used rather than circles to properly handle out-of-plane rotation.

A naive approach to iris ellipse estimation would be to use the points near the boundary of the iris. However, the shape of the iris segmentation may at this point be very different from elliptical, and the iris may be occluded partly by the eyelashes (on the top or bottom or both). For reliable initial estimate of iris boundary points, we extend rays from the pupil center in a manner similar to that described previously in order to find locations where the rays transition from an iris region to the background region. Because some of these rays may not lead to an iris boundary point, only a subset of the 360 points is obtained. To increase the number of points (and hence increase the reliability of the ellipse fitting procedure), we utilize the inherent symmetry of the iris region. For each ellipse point, a new point is generated about the vertical symmetry line passing through the center of the iris, if a point does not already exist for that direction. In addition, points whose distance from the pupil center exceeds 1.5 times the distance of the closest point to the pupil center are rejected. If this does not yield a sufficient number of points, horizontal symmetry of the ellipse is used to duplicate the iris points. This procedure yields a substantial set of points to which an ellipse is fit using the least squares method proposed by Fitzgibbon et al. [13]. The assumption that the iris is symmetric and the pupil and the iris centers are close to each other may not always be true leading to outliers. Embedding the fitting method within a RANSAC algorithm [12] yields additional robustness in the presence of outliers. Fig. 7 illustrates the procedure and the resulting improvement.

5. Experimental results

Two databases were utilized to evaluate the effectiveness of the proposed iris segmentation algorithm in dealing with non-ideal iris

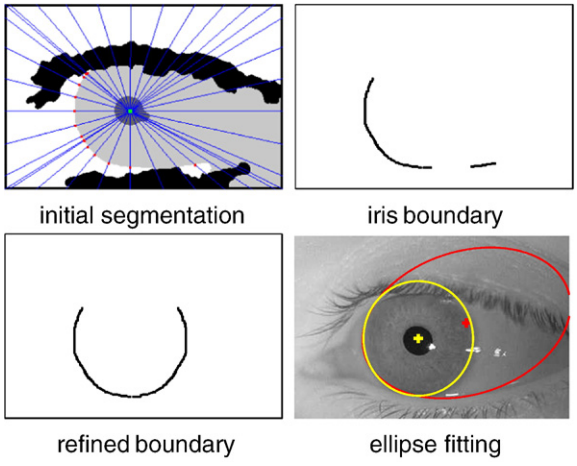

Fig. 7. Refining the iris segmentation. Top left: Iris segmentation image with pupil center overlaid (green dot). The lines originating from the center point in 360° of the center point intersect with the iris boundary at points shown in red. For clarity only a subset of lines and corresponding points are shown. Top right: Potential iris boundary points. Due to erroneous segmentation, the full set of points is not obtained. Bottom left: Increasing the iris boundary points using the pupil center and the inherent symmetry in the iris regions. Bottom right: Ellipse fitting to the potential iris boundary points leads to an erroneous result (red ellipse), while fitting to the increased boundary points leads to the correct result (yellow ellipse).

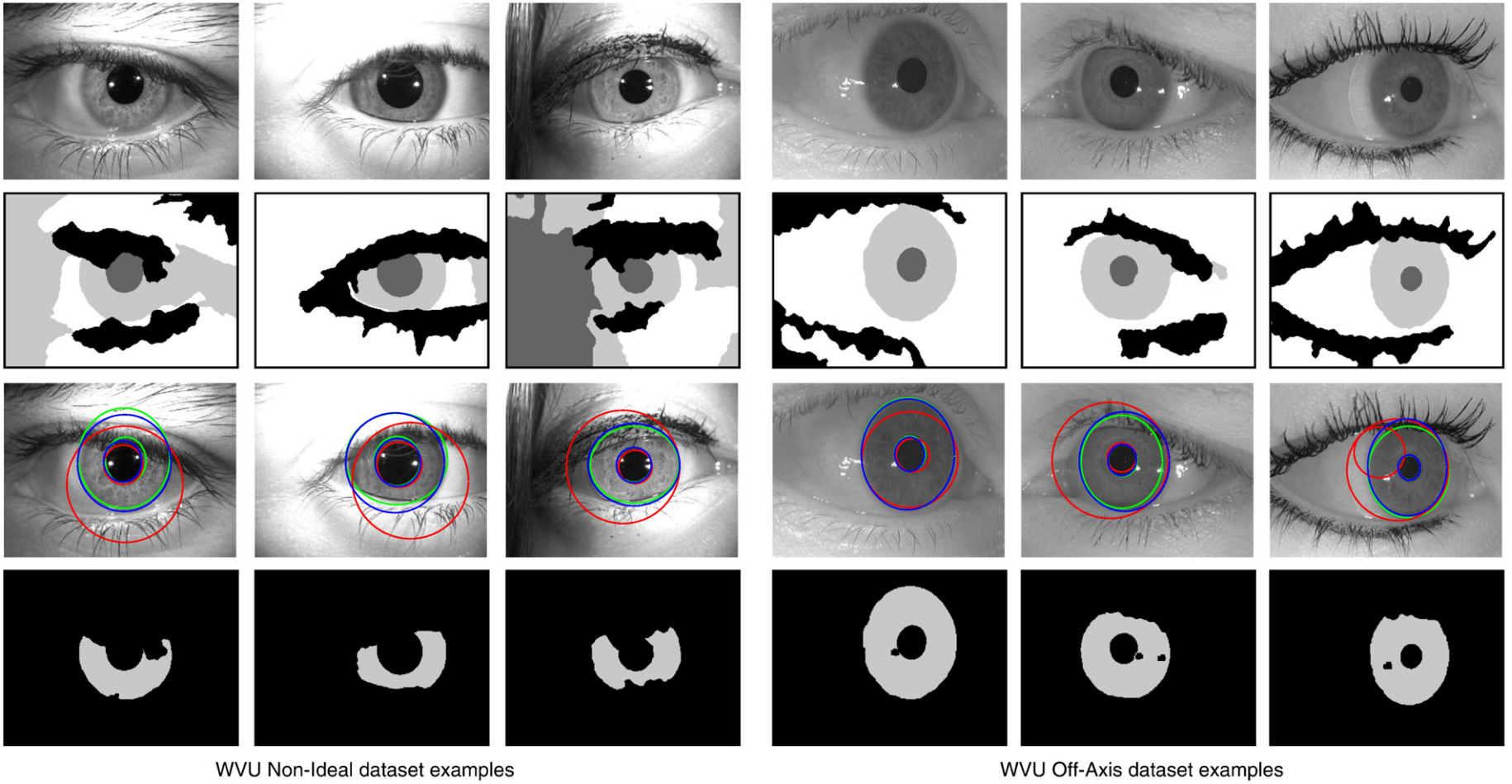

Fig. 8. Results of our algorithm on example images from the two databases with first row showing the example images, followed by the preliminary segmentation, the estimated iris shape, and the segmented iris mask which is obtained after combining the results in the second and the third rows. The segmentation shows four regions: pupil (dark gray), iris (light gray), eyelashes (black), and background (white). In the third row, notice that the resulting pupil and iris ellipses obtained by our algorithm (blue) are more accurate and closely aligned to the iris than those obtained by the edge-based algorithm (green), or algorithm of [22] (red), which is distracted by the eyelashes and the non-circularity of the iris. The iris mask is used for recognition.

Table 1
Characteristics of the 200 manually labeled images from the WVU Non-Ideal and Off-Axis databases.

Parameter	100 non-ideal images			
	Average	Max.	Min.	Std.
Iris area (pixels)	24,692	38,315	14,000	5693
Pupil area (pixels)	4244	14,175	1231	2520
Iris occlusion (%)	27	54	3	13
Eccentricity	1.01	1.14	0.9	0.05
Iris intensity variation	26	49	10	9
Parameter	100 off-axis images			
	Average	Max.	Min.	Std.
Iris area (pixels)	33,155	42,380	22,381	4622
Pupil area (pixels)	3764	10,807	1508	1585
Iris occlusion (%)	11	35	0	8
Eccentricity	1.08	1.3	1.0	0.06
Iris intensity variation	10	16	7	2

Table 2
Comparison of our segmentation algorithm, an edge-based segmentation approach, and Masek's implementation of Daugman's algorithm, using the ground truth data for 100 images each from the WVU Non-Ideal (NI) and WVU Off-Axis (OA) iris database. The lowest error is shown in bold.

Parameter	Average error/standard deviation (in pixels)					
	Our algorithm		Edge-based segmentation		Masek [22]	
	NI	OA	NI	OA	NI	OA
Iris center (x)	**2.1/.6**	**2.3/2.8**	5.8/12.5	4.5/10.2	10.1/15.2	7.1/14.2
Iris center (y)	**3.0/2.4**	**2.0/2.7**	5.5/6.8	3.6/3.3	7.3/9.2	4.1/6.4
Iris radius (x)	**2.8/3.6**	**3.0/3.2**	6.0/13.5	6.7/14.6	6.1/7.2	5.1/6.0
Iris radius (y)	**4.4/4.6**	**3.5/3.2**	8.7/9.0	3.7/4.5	6.4/7.1	4.0/3.4
Pupil center (x)	**0.9/1.3**	**1.0/1.2**	2.4/14.9	1.2/2.4	5.0/10.1	2.8/14.3
Pupil center (y)	0.7/1.5	0.8/1.5	**0.6/0.9**	**0.6/0.7**	3.7/6.6	2.0/1.6
Pupil radius (x)	**1.5**/1.9	**1.4**/1.3	1.7/**1.7**	1.5/**1.1**	3.7/5.0	2.5/1.8
Pupil radius (y)	**1.2**/**1.8**	**1.2**/1.4	1.4/2.4	1.5/**0.9**	3.6/5.0	1.8/1.6
Pixel labels	**15%/10%**	**6%/6%**	37%/27%	18%/27%	55%/41%	16%/21%

images. The WVU Non-Ideal iris database from West Virginia University is part of a larger multi-modal biometric database [7]. It contains several thousand images from 244 subjects captured by a near infra red camera. Of these subjects, 227 had both eyes captured, 8 had only the left eye captured, and 5 had only the right eye captured. This yields a total of 467 individual eyes (235 left and 232 right) represented in the database. Since a variable number of images were captured for each eye (between 4 and 15, inclusive), we retain exactly four images per eye (the minimum number), leading to a total of 1868 images, to enforce consistency and alleviate the potential of bias in the results. The images were taken from a variety of distances from the subject with changing illumination conditions, blurring, and significant amount of iris occlusion by eyelashes. The WVU Off-Axis database available from the same researchers comprises 584 images belonging to 73 subjects. There are eight images per subject, two images of each eye captured on-axis, and two images of each eye captured off-axis. Treating each eye as a separate class, the database can be considered as containing 146 classes with 4 images per class.

The results of our algorithm on several images from these databases are shown in Fig. 8. The experiments were carried out using the following parameters: $\tau = 50$ (threshold on texture strength), $\sigma = 5$ (texture smoothing factor), and $\kappa = 0.75$ (search range for iris boundary). In all cases, the four regions are segmented accurately, and an ellipse is well-fitted to both the iris and the pupil. In addition, an iris mask is generated by retaining only the pixels in the iris region that also lie within the iris ellipse, as well as by discarding pixels detected to be specular reflections by the preprocessing step. The mask is used in iris recognition, described later. Our algorithm is compared with the publicly available implementation of Daugman's algorithm by Masek [22]. In addition, to demonstrate the effectiveness of the pixel-level segmentation of we developed an edge-based segmentation algorithm in which an ellipse is fitted to the points defined by the intensity edges separating the iris region from the pupil and the background. The iris region mask for this edge-based algorithm is determined by the eyelash mask produced by Masek [22]. Comparing these results with the traditional geometry based approach reveals the importance of the pixel-level segmentation in obtaining an accurate ellipse. Note the same parameters were used for all results presented in this section. Segmentation results of our approach on some example images from the ICE database are shown in Fig. 9.

To provide quantitative results measuring the accuracy of our segmentation, we selected the first 25 eyes from each of the datasets, and four images per eye. In each of these 200 images, we manually labeled the iris pixels by drawing ellipses around the pupil and iris, then painting the individual pixels to eliminate specular reflections as well as occlusions by eyelids and eyelashes. The ellipses enclosing the iris and pupil were drawn by manually specifying the extremities of the major and minor axes. Table 1 lists the various parameters of the extracted ground truth data. In comparison to the off-axis dataset, the non-ideal dataset shows a higher variability of iris and pupil area, intensity values of iris pixels, and the iris area occluded by the eyelashes and specular reflections. On the other hand, the iris regions in the off-axis dataset are more eccentric due to the out-of-plane rotation of the iris.

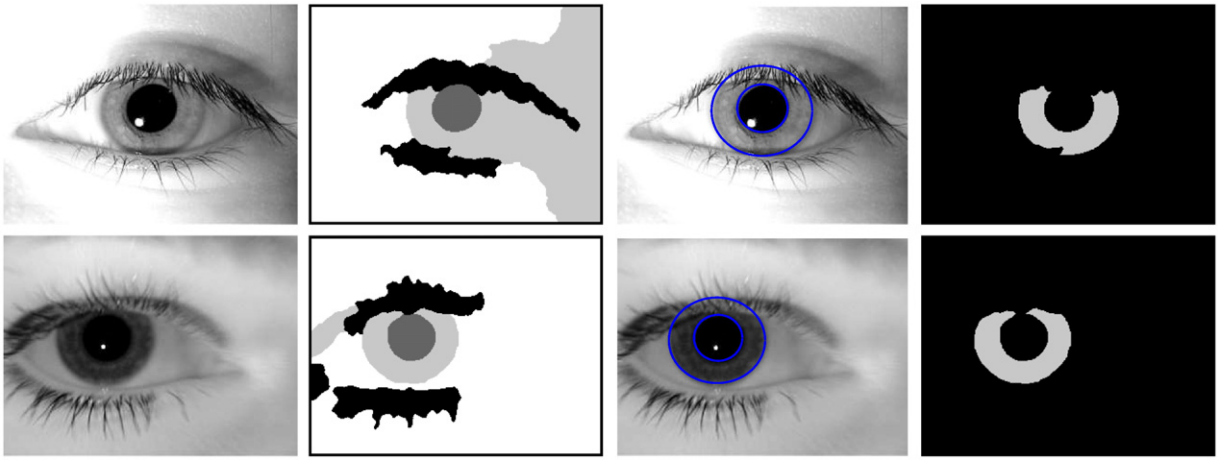

Fig. 9. Results of our algorithm on two example images from the ICE dataset with first column showing the example images, followed by the preliminary segmentation, the estimated iris shape, and the segmented iris mask which is obtained after combining the results in the second and the third columns.

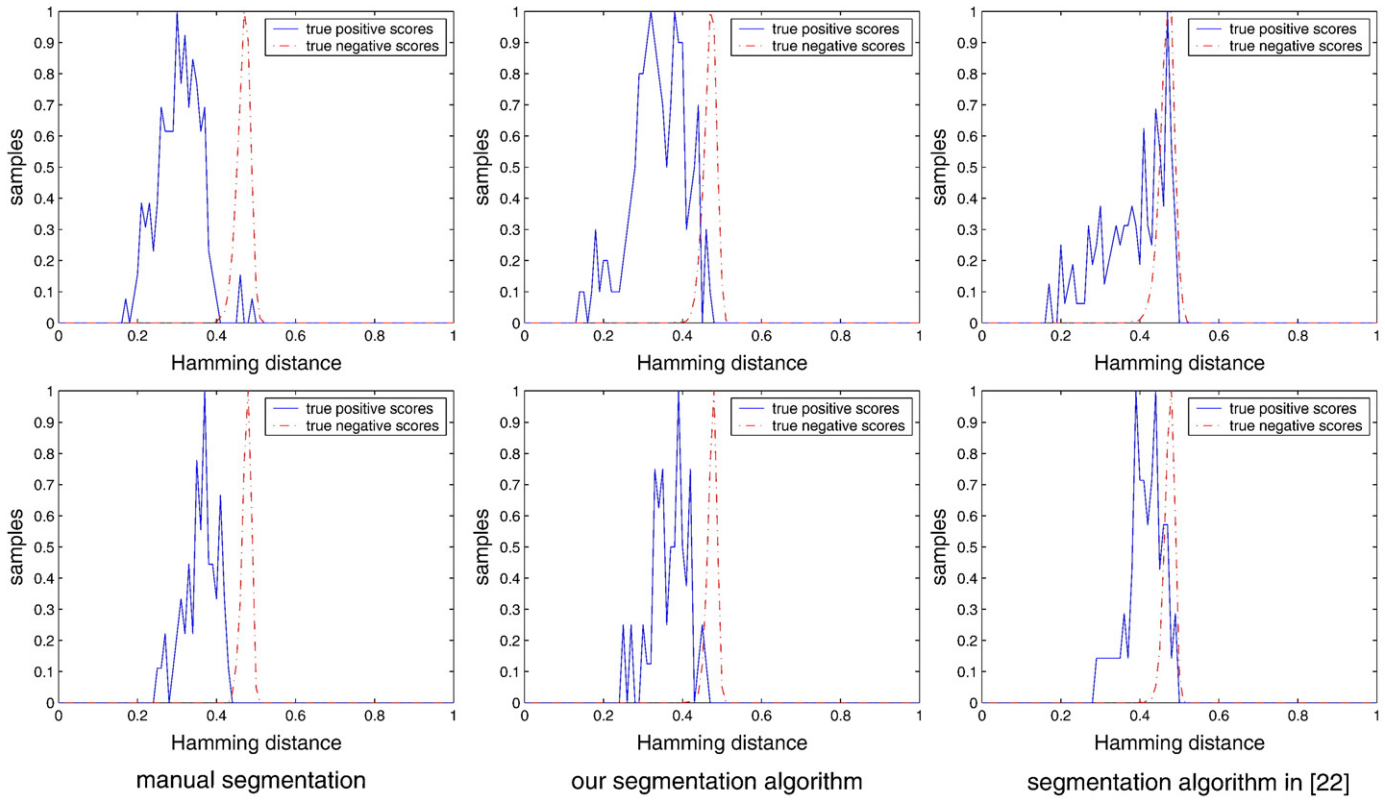

Fig. 10. Match score distribution for three approaches for 100 iris images each from WVU Non-Ideal Iris database (top row) and WVU Off-axis database (bottom row) belonging to 25 classes with 4 samples each. Similar to manual segmentation, our algorithm is able to achieve a clear separation between genuine matches and false matches, whereas Masek [22] is not.

The results of our algorithm on these 200 images, compared with the manually labeled ground truth, are shown in Table 2 for the non-ideal and off-axis database. We measured both the percentage of mislabeled iris pixels (number of pixels in the iris mask that do not match the ground truth mask normalized by the number of pixels in the ground truth mask), as well as the error in the parameters of the estimated pupil and iris ellipses. Our algorithm clearly outperforms [22] and the edge-based algorithm, achieving a segmentation error of 15% and 6% on the two databases, and computing an ellipse with an error not exceeding 3 pixels in nearly all the measured parameters. It can be seen that while our segmentation errors on the Off-Axis database are less than those of the Non-Ideal database, the accuracy of the ellipse parameters is about the same. The computation time required for obtaining the initial segmentation and the refined iris estimate is 5 sec. and 3 sec. respectively using an unoptimized C++ implementation. Computational efficiency was not the primary goal while developing the algorithm. Optimization of the code can be carried out to reduce the algorithm run time and is left as future work.

The proposed algorithm is further validated by considering the improvement obtained in iris recognition. In this work we do not develop new procedures for matching two segmented iris regions for recognition. Instead, we used Masek's publicly available implementation of the Daugman's algorithm [22] to perform the iris unwrapping and iris template matching. We modified this code to accept our iris segmentation mask as input. Also, since the code assumes that the iris region is circular, we transformed our elliptical iris to a circle by either using an affine transform (ellipse warping) or just using the minimum values of the x and y radii of the ellipse as the radius of the circle (no ellipse warping). Fig. 10 depicts the match score distribution for subsets of the non-ideal and off-axis databases using

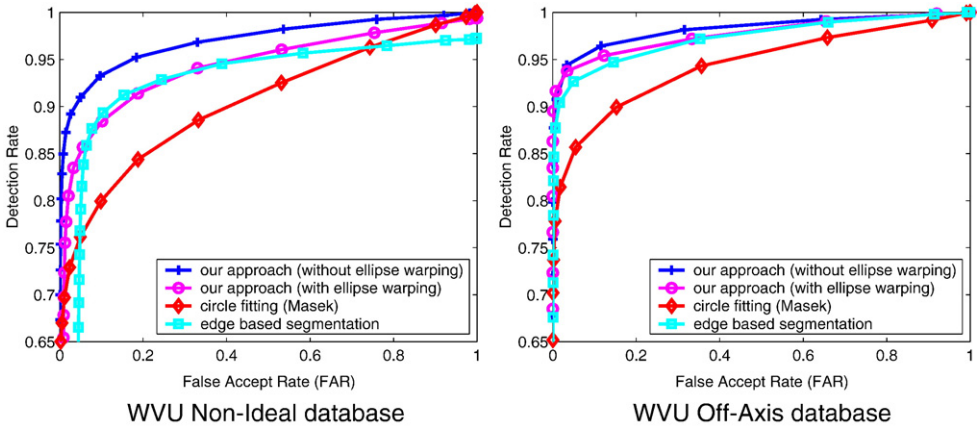

Fig. 11. ROC curves for iris recognition using various segmentation algorithms on the two databases (Non-Ideal and Off-Axis with 1868 and 584 images, respectively).

Table 3
Equal error rates (EERs) for iris recognition performed using various segmentation algorithms on the WVU Non-Ideal and WVU Off-Axis databases.

Segmentation approach	WVU Non-Ideal Iris database (1868 images)	WVU Off-Axis Iris database (584 images)
Our algorithm (w/o ellipse warping)	**0.082**	**0.045**
Our algorithm (w/ ellipse warping)	0.108	0.048
Edge based	0.105	0.062
Masek [22]	0.172	0.127

three different iris segmentation approaches: ground truth segmentation, our algorithm, and the Masek implementation. Notice that the distribution (Hamming distance) obtained by our algorithm is close that obtained using ground truth segmentation, whereas there is a significant amount of overlap between the true positive and the true negative scores for the Masek code.

Receiver Operating Characteristic (ROC) curves for various algorithms are shown in Fig. 11, which compares our algorithm (both with and without ellipse warping), the implementation of Masek [22], and the edge-based segmentation algorithm described earlier. Evaluated on the larger versions of WVU Non-Ideal and Off-Axis databases, our algorithm performs recognition with significantly higher accuracy than the other algorithms. Equal error rates (EERs) are shown in Table 3. In general, results are better without ellipse warping, which reflects the trade off between the greater expressiveness of the ellipse model and the greater stability of the circle model. Since the non-ideal images were captured head-on, and many of the off-axis images were also captured without much out-of-plane rotation, the added benefit of the ellipse model is offset by the greater sensitivity to noise. We conclude from these data that while the ellipse model is necessary to achieve accurate recognition, it may not be reliable enough to perform the delicate operation of affine warping. An implicit assumption while using a parametric model like an ellipse is that the iris boundary is circular in the plane, which may not be necessarily true due to small local deviations. In contrast to the active contour based approaches for modeling the exact non-circular boundary [10,24,26], our approach features a pixel-level region mask that preserves the local variations, and the corresponding parametric curve (ellipse) that can be used for unwrapping and normalization. Hence, the final iris region mask is obtained as a result of both of these complementary processes.

To our knowledge, of the previous approaches dealing with non-ideal iris images mentioned in this paper, only two report iris recognition results on the WVU Non-Ideal and WVU Off-Axis databases. Shah and Ross [26] perform recognition separately on the left and the right eyes of the WVU Non-Ideal dataset, reporting EERs of 0.142 and 0.12, respectively. The WVU Off-axis database was used for testing the approach presented by Schuckers et al. [25], where EERs of 0.0001, 0.003, and 0.08 were reported while performing recognition of three different eye orientations (estimation of the gaze angle was performed automatically). Comparing these numbers to EERs obtained using our approach (shown in Table 3), it can be seen that our approach achieves better performance than [26], but performs considerably worse than [25]. However, because of the differences in the experimental details in these previous approaches, we should be cautious in interpreting these results. There are three major differences. First, there is a difference in the number of images used

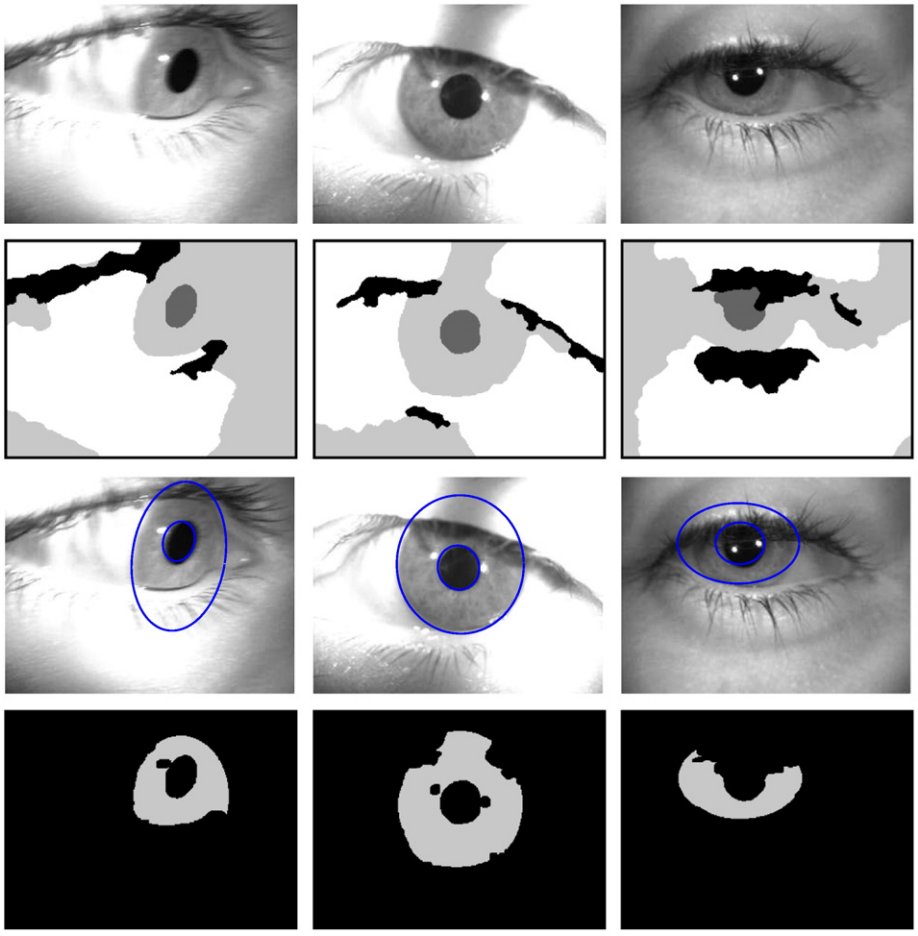

Fig. 12. Failure cases. Some examples where inaccurate segmentation is obtained on account of (left to right) segmentation and ellipse estimation error, pixel labeling error, and segmentation error due to low contrast between iris and background regions.

for the experiments. While using the WVU Non-Ideal dataset, [26] reports results on 2786 total iris images, whereas we use 1868 images (to ensure the same number of images per class). While using the WVU off-Axis dataset, [25] reports results on 800 images, while we use 584 images (all the images available to us). Secondly, there is a difference in the experimental setup. In the case of WVU Non-Ideal dataset, [26] compares left and right iris separately. A larger difference exists in the case of [25], where experiments are carried out based on three different eye orientations. Our approach in contrast reports the overall recognition performance in each case. Thirdly, the focus of our approach is on iris segmentation and we do not propose any advances in the iris encoding steps. We use the existing code from [22] to perform iris encoding and normalization which are the key steps in recognition. Due to the above reasons a direct comparison to the previous approaches is not feasible, although it is our belief that the recognition results obtained due to our segmentation can be further improved by using an improved encoding algorithm. Such an exploration is left for future work.

In this work, we only present iris segmentation results in the NIR images. Another limitation of the formulation restricts the algorithm from dealing with large in-plane rotations of the eye while performing recognition. The test cases involve a large out-of-plane rotation but a small amount of relative in-plane rotation in most classes. The segmentation depends upon the presence of texture around the eyelashes and grayscale intensity differences in the iris, pupil, and the background regions. In some cases, lack of sufficient texture leads to errors in segmentation of the eyelashes. Also, in some images, parts of the background and the iris are merged due to the closeness of the grayscale values associated with the corresponding regions. Some failure cases are shown in Fig. 12. Other reasons of failure of the algorithm include low contrast iris images, near total occlusion of the iris region, and the presence of highly textured spots within the iris regions.

6. Conclusion

This paper presents a novel approach for non-ideal iris segmentation using graph cuts and demonstrates its effectiveness in terms of iris segmentation and recognition. Our approach combines region based cues such as intensity and coarse texture with image gradients and eye geometry heuristics to perform iris segmentation. A key component of the approach is a dense graph cuts-based segmentation technique which uses both texture and intensity to segment non-ideal iris images into four regions: iris, pupil, eyelashes, and background. The algorithm is able to handle multi-modal distributions of intensities in iris and background regions. One of the chief advantages of performing explicit segmentation is the ability to account for the occlusion of the iris by the eyelids and eyelashes. The iris masks thus obtained are compared with ground truth data for the iris regions extracted from various non-ideal iris image databases demonstrating the accuracy of our approach. Further validation of our segmentation algorithm is performed via iris recognition over these databases. Future work should focus on incorporating shape prior in iris segmentation, more precise modeling of eyelashes to yield refined occlusion masks, estimation of in-plane rotation of the eye, testing the segmentation on images from visual spectrum, as well as algorithm optimization by exploring the use of efficient solvers than the alpha-beta swap to enable real-time performance.

References

[1] A. Bachoo, J. Tapamo, Texture detection for segmentation of iris images, Annual Research Conference of the South African Institute of Computer Information Technologies (2005) 236–243.
[2] K. Bowyer, K. Hollingsworth, P. Flynn, Image understanding for iris biometrics: a survey, Journal of Computer Vision and Image Understanding 110 (2) (2007) 281–307.
[3] Y. Boykov, V. Kolmogorov, An experimental comparison of min-cut/max-flow algorithms for energy minimization in vision, IEEE Transactions on Pattern Analysis and Machine Intelligence 26 (9) (2004) 1124–1137.
[4] Y. Boykov, O. Veksler, R. Zabih, Fast approximate energy minimization via graph cuts, IEEE Transactions on Pattern Analysis and Machine Intelligence 23 (11) (2001) 1222–1239.
[5] T. Camus, R. Wildes, Reliable and fast eye finding in close-up images, Proceedings of the IAPR International Conference on Pattern Recognition, 2002, pp. 389–394.
[6] D. Comaniciu, V. Ramesh, P. Meer, Kernel-based object tracking, IEEE Transactions on Pattern Analysis and Machine Intelligence 25 (5) (May 2003) 564–577.
[7] S.G. Crihalmeanu, A.A. Ross, S.A. Schuckers, L.A. Hornak, A Protocol for Multi-biometric Data Acquisition, Storage and Dissemination. Tech. Rep., Lane Department of Computer Science and Electrical Engineering, West Virginia University, 2007.
[8] J. Daugman, High confidence visual recognition of persons by a test of statistical independence, IEEE Transactions on Pattern Analysis and Machine Intelligence 15 (11) (1993) 1148–1161.
[9] J. Daugman, Statistical richness of visual phase information: update on recognizing persons by iris patterns, International Journal of Computer Vision 45 (1) (2001) 23–38.
[10] J. Daugman, New methods in iris recognition, IEEE Transactions on Systems, Man, and Cybernetics. Part B: Cybernetics 37 (5) (2007) 1167–1175.
[11] X. Feng, C. Fang, X. Ding, Y. Wu, Iris localization with dual coarse to fine strategy, Proceedings of the IAPR International Conference on Pattern Recognition, 2006, pp. 553–556.
[12] M.A. Fischler, R.C. Bolles, Random sample consensus: a paradigm for model fitting with applications to image analysis and automated cartography, Communications of the ACM 24 (6) (1981) 381–395.
[13] A.W. Fitzgibbon, M. Pilu, R.B. Fisher, Direct least-squares fitting of ellipses, IEEE Transactions on Pattern Analysis and Machine Intelligence 21 (5) (May 1999) 476–480.
[14] Z. He, T. Tan, Z. Sun, Iris localization via pulling and pushing, Proceedings of the IAPR International Conference on Pattern Recognition, 2006, pp. 366–369.
[15] J. Huang, Y. Wang, T. Tan, J. Cui, A new iris segmentation method for recognition, Proceedings of the IAPR International Conference on Pattern Recognition, 2004, pp. 368–872.
[16] B. Kang, K. Park, A robust eyelash detection based on iris focus assessment, Pattern Recognition Letters 28 (13) (Oct. 2007) 1630–1639.
[17] W. Kong, D. Zhang, Detecting the eyelash and reflection for accurate iris segmentation, International Journal of Pattern Recognition and Artificial Intelligence 17 (6) (2003) 1025–1034.
[18] D. Li, D. Winfield, D. Parkhurst, Starburst: a hybrid algorithm for video based eye tracking combining feature based and model based approaches, Workshop on Vision for Human Computer Interaction, CVPR, 2005.
[19] X. Liu, K. Bowyer, P. Flynn, Experiments with improved iris segmentation algorithm, Fourth IEEE Workshop on Automatic Identification Technologies, 2005, pp. 118–123.
[20] L. Ma, T. Tan, Y. Wang, D. Zhang, Personal identification based on iris texture analysis, IEEE Transactions on Pattern Analysis and Machine Intelligence 25 (12) (2003) 1519–1533.
[21] L. Ma, T. Tan, Y. Wang, D. Zhang, Efficient iris recognition by characterizing key local variations, IEEE Transactions on Image Processing 13 (6) (2004) 739–750.
[22] L. Masek, P. Kovesi, Matlab Source Code for a Biometric Identification System based on Iris Patterns. Tech. Rep., The School of Computer Science and Software Engineering, The University of Western Australia, 2003 http://www.csse.uwa.edu.au/pk/studentprojects/libor/sourcecode.html.
[23] S. Pundlik, D. Woodard, S. Birchfield, Non-ideal iris segmentation using graph cuts, Proceedings of the IEEE Computer Society Workshop on Biometrics (in association with CVPR), 2008.
[24] A. Ross, S. Shah, Segmenting non-ideal irises using geodesic active contours, Proceedings of Biometrics Symposium, 2006.
[25] S. Schuckers, N. Schmid, A. Abhyankar, V. Dorairaj, C. Boyce, L. Hornak, On techniques for angle compensation in nonideal iris recognition, IEEE Transactions on Systems, Man, and Cybernetics. Part B: Cybernetics 37 (5) (2007) 1176–1190.
[26] S. Shah, A. Ross, Iris segmentation using geodesic active contours, IEEE Transactions on Information Forensics and Security 4 (4) (2009) 824–836.
[27] J. Shi, C. Tomasi, Good features to track, Proceedings of the IEEE Conference on Computer Vision and Pattern Recognition (CVPR), 1994, pp. 593–600.
[28] M. Vatsa, R. Singh, A. Noore, Improving iris recognition performance using segmentation, quality enhancement, match score fusion, and indexing, IEEE Transactions on Systems, Man, and Cybernetics. Part B: Cybernetics 38 (4) (2008) 1021–1035.
[29] R. Wildes, Iris recognition: an emerging biometric technology, Proceedings of IEEE 85 (9) (1997) 1348–1363.
[30] G. Xu, Z. Zhang, Y. Ma, Improving the performance of iris recognition systems using eyelids and eyelash detection and iris image enhancement, Proceedings of 5th International Conference on Cognitive Informatics, 2006.